34th Annual International Conference of the IEEE EMBS
San Diego, California USA, 28 August - 1 September, 2012

Implant Positioning System Using Mutual Inductance

You Zou[1] and Stephen O'Driscoll[1]

Abstract— **Surgical placement of implantable medical devices (IMDs) has limited precision and post-implantation the device can move over time. Accurate knowledge of the position of IMDs allows better interpretation of data gathered by the devices and may allow wireless power to be focused on the IMD thereby increasing power transfer efficiency. Existing positioning methods require device sizes and/or power consumptions which exceed the limits of in-vivo *mm*-sized IMDs applications. This paper describes a novel implant positioning system which replaces the external transmitting (TX) coil of a wireless power transfer link by an array of smaller coils, measures the mutual inductance between each coil in the TX array and the implanted receiving (RX) coil, and uses the spatial variation in those mutual inductances to estimate the location of the implanted device. This method does not increase the hardware or power consumption in the IMD. Mathematical analysis and electromagnetic simulations are presented which explain the theory underlying this scheme and show its feasibility. A particle swarm based algorithm is used to estimate the position of the RX coil from the measured mutual inductance values. MATLAB simulations show the positioning estimation accuracy on the order of 1 *mm*.**

I. INTRODUCTION

A number of implant positioning systems (IPS) have been presented in the literature. Most generate a signal at the implanted medical device (IMD) and use distributed receivers outside the body to sense that signal and then estimate the location of the IMD by triangulating the signals received from the source. In [1] the implanted signal source is a DC magnet which has the drawback of occupying too large a volume for many applications; while in [2] the implanted signal source is an RF transmitter which consumes a large amount of power at the implant site. [3] attempts to overcome these problems by transmitting a signal from an array of external transmitters to a coil on the implanted device and estimating the location of the implanted device by the strength of each signal received. This scheme however requires additional circuitry and power consumption at the IMD.

In this paper, a novel implant positioning method based on mutual inductance, M, is presented. The external transmitting (TX) coil of a wireless power transfer link is replaced by an array of smaller coils. When power is transmitted electromagnetically from the external TX array to the implanted RX coil a time-varying current is induced in the RX coil. This current in the RX coil generates another weaker electromagnetic field which will be sensed by the TX array coils. This allows the mutual inductance, M_i, between each coil in the TX array and the RX coil to be measured, and the spatial variation in those mutual inductances is then used to estimate the location of the implanted device. This method does not increase the hardware or power consumption in the IMD, instead all additional circuitry and power consumption is located at the external device whose area and power constraints are much more relaxed. Therefore this approach is much more attractive for *mm*-sized IMDs applications such as in [4].

This paper first describes the theoretical basis and feasibility of the proposed IPS by examining the variation of mutual inductance between two coils with relative location and orientation and by demonstrating the location for the RX coil can be found via a lookup table approach. Secondly an algorithm based on the Particle Swarm Optimizer (PSO) is presented as an alternative to the lookup table approach to solve for the RX coil position given the set of M_i's. Finally MATLAB simulations results which show the positioning accuracy of this algorithm to be on the order of 1 *mm* are presented.

II. THEORETICAL FEASIBILITY OF PROPOSED IPS

A. Spatial Dependence of Mutual Inductance

The mutual inductance, M, between two coils, C_r and C_t, of arbitrary location and orientation is given by the Neumann Integral in Eq. (1). The subscripts t and r denote the TX and RX coil respectively.

$$M_{tr} = \frac{\mu_0}{4\pi} \oint_{C_t} \oint_{C_r} \frac{d\underline{s_r} \cdot d\underline{s_t}}{|\underline{r_{tr}}|} \tag{1}$$

where μ_0 is the permeability in free space, $\underline{s_i}$ is the incremental vector tangential to the circumference of coil i, and $|r_{tr}|$ is the distance between $\underline{s_t}$ and $\underline{s_r}$. The Neumann Integral allows us to explore the variation of M with the horizontal displacement ρ, vertical displacement d, and orientation of the RX coil. The orientation can be described by θ and ϕ, the angles used in conventional spherical coordinates. Fig. 1 illustrates the location and orientation of one coil with respect to the other whose axis is assumed parallel to the Z-axis.

Fig. 2 illustrates the variation of M with ρ and d using both MATLAB solution of Eq. (1) and electromagnetic simulations using Agilent's ADS Momentum. The results agree closely deviating slightly since octagonal antennas of finite width and thickness are simulated in Momentum while the Neumann Integral considers two circular filaments. For example when d = 15 *mm*, as ρ increases, M first decreases to a negative minimum and then asymptotically approaches

[1]You Zou and Stephen O'Driscoll are with Solid-State Circuits Research Lab, Department of Electrical and Computer Engineering at the University of California, Davis, One Shields Avenue, Davis, CA 95616, USA {youzou, odriscoll} at ucdavis.edu

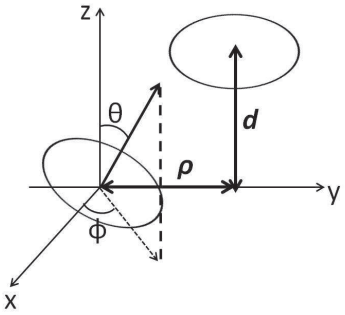

Fig. 1. Coil spatial parameters illustration.

zero, a non-monotonic characteristic. As d increases, M goes to zero asymptotically from a positive maximum when ρ is small (e.g. 10 *mm*); while M increases to a positive maximum from a negative minimum and then asymptotically approaches zero when ρ is big enough (e.g. 20 *mm*). The variation of M with θ is very close to a sinusoid with a period of 2π; while the period and shape of the variation with ϕ depends on θ, d and ρ. Therefore many positions and orientations will result in the same M and so there is not a one-to-one mapping between position and M. Specifically given M and the transmitter location and orientation we would not have enough information to say where the RX coil is located i.e. the Neumann Integral is not invertible. However we could narrow the set of possible locations down to a particular set given that information. If we have N such TX coils with known positions and we know the M_i between each TX coil and the RX coil then we have N such restricted sets which describe the possible locations of the RX coil. The RX coil must lie in the intersection of those sets and so as N increases we hope to narrow down the location of the RX coil to a point.

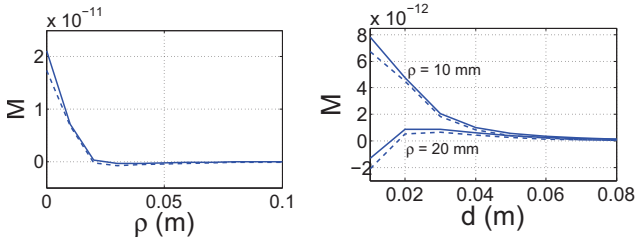

(a) (b)

Fig. 2. Spatial Variation of M when radius of coils = 2.5 *mm*. Solid line is obtained using MATLAB. Dashed line is obtained using ADS Momentum. (a) M vs. ρ. $\phi_r = \theta_r = \phi_t = \theta_t = 0^o$. d = 15 *mm*. (b) M vs. d at different ρ's. $\phi_r = \theta_r = \phi_t = \theta_t = 0^o$.

B. Estimating Location from Mutual Inductances

To demonstrate the feasibility of estimating the RX coil location from the measured M_i's and to examine the number of TX coils required, N, we consider a look-up table approach to inverting the Neumann Integral. Consider first the simplified case of one TX coil is parallel to one RX coil and both coils parallel to the XY-plane so that there are only two free variables, ρ and d. In the look-up table approach we pre-calculate the mutual inductance between the TX coil and RX coil, M_{calc}, for all possible RX coil locations. Due to symmetry and the non-monotonic nature of the spatial variation of M, there will be a number of different locations of the RX coil which give the same M for a fixed TX coil. This is shown in Fig. 3, which depicts the contour plot of $log_{10}(|M_{calc}|)$ vs. ρ and d, where both ρ and d are in meters. This constitutes a 2D look-up table of M_{calc}'s in which each M_{calc} corresponds to a number of different combinations of d's and ρ's.

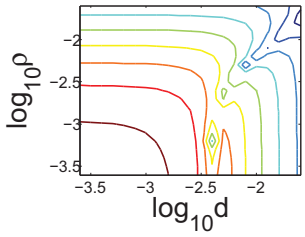

Fig. 3. Contour plot of $log_{10}(|M_{calc}|)$ vs. vertical displacement d and horizontal displacement ρ for $\phi_r = \theta_r = \phi_t = \theta_t = 0^o$ and radius of coils = 2.5 *mm*.

If one TX coil is used and the mutual inductance between it and the RX coil, M_1, is measured, the possible $\rho - d$ pairs for the RX coil location can be identified by scanning through the look-up table and searching for every combination of $\rho - d$ pairs corresponding to an M_{calc} equivalent or close enough to the M_1. If a second TX coil is added next to the existing one, then a second mutual inductance M_2 can be measured between it and the RX coil. A second possible set of $\rho - d$ pairs for the RX coil location can then be identified by scanning through the look-up table and searching for every combination of $\rho - d$ pairs corresponding to an M_{calc} equivalent or close enough to the M_2 as before. The intersection of both sets of possible $\rho - d$ pairs is a smaller set and gives all possible locations. As we add more TX coils, the number of possible locations of the RX coil will continue to decrease. Fig. 4, for which the mutual inductances were found by ADS momentum simulation, demonstrates the trend by showing the narrowing down of possible $\rho - d$ pairs for RX coil location when N increases from two to four. The markers in Fig. 4 represent the overlapped $\rho - d$ pairs for the RX coil location at a pre-defined position where it is assumed that the ρ and d each lie between 0 and 5*cm*. In reality the look-up table has five dimensions x, y,[1] d, θ_r and ϕ_r. The location and orientation of the RX coil can then be similarly found but only if a sufficiently large N is employed. Investigating how the minimum required N varies with the accuracy required and the transmit array layout is ongoing. The look-up table approach is straightforward to implement

[1]earlier we considered $\rho = \sqrt{x^2 + y^2}$ as the X and Y axes locations within the given XY-plane are arbitrary when only two circular coils, coaxial on Z, are used.

but becomes quite costly in terms of area and power for high resolution.

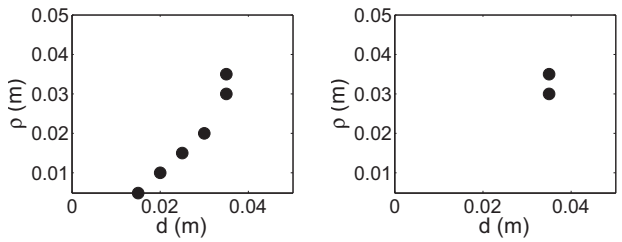

Fig. 4. Illustration of intersection of possible sets of ρ-d pairs for $\phi_r = \theta_r = \phi_t = \theta_t = 0^o$ and radius of coils = 2.5 *mm* using (a) Two TX coils. (b) Four TX coils.

III. Position Estimation Algorithm

A. Problem Formulation

Computing and storing a lookup table costs significant power and area. One algorithmic approach to finding the RX position is to transform the problem to an optimization problem. Specifically find the RX coil location and orientation which minimizes:

$$\sum_{i=1}^{N}(M_{i,meas} - M_{i,calc})^2 \tag{2}$$

where M_i is the mutual inductance between the i^{th} transmit coil and the RX coil for each of the N TX coils. $M_{i,meas}$ is the measured mutual inductance and $M_{i,calc}$ is calculated as a function of RX coil location and orientation. Since the solution space has many local minima, some conventional nonlinear optimization algorithms such as Levenberg-Marquardt, etc. would require a very good initial guess of the solution [5], which makes them not suitable for applications with little indication of RX coil position beforehand. Therefore, an algorithm based on the particle swarm optimizer (PSO), a metaheuristic algorithm, is presented to demonstrate the positioning process.

B. Particle Swarm Optimization

Similar to the process of a swarm of insects searching for food [6], in this case a swarm of particles search for the location and orientation of the RX coil which will minimize (2). Searching trajectories of each particle are based on their personal experience, evaluated by the personal fitness function, as well as the overall satisfaction level of the entire swarm, which can be found after evaluating the global fitness function for each particle. The personal and global fitness functions are given by (3) and (4) respectively.

$$\sum_{i=1}^{N}(M_{i,meas} - M_{i-p,calc})^2 \tag{3}$$

$$\sum_{i=1}^{N}(M_{i,meas} - M_{i-p_{best},calc})^2 \tag{4}$$

where $M_{i-p,calc}$ is the M calculated between the i^{th} TX coil and the RX coil placed at the current location of the p^{th} particle. Among all previous locations that the p^{th} particle has flown over, the one that gives the smallest value evaluated by (3) is used to calculate $M_{i-p_{best},calc}$ in (4).

C. Problem Reformulation to Exploit Symmetries

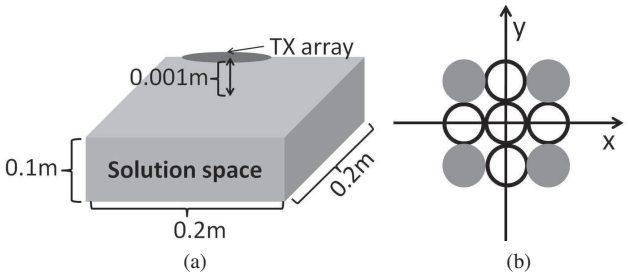

Fig. 5. (a) Simulation system setup (b) A nine-TX coil array. Shaded coils are the corner coils. Radius of coils = 2.5 *mm*. $\phi_r = \theta_r = \phi_t = \theta_t = 0^o$.

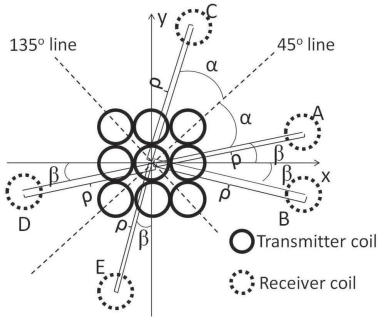

Fig. 6. Typical symmetric points in the XY-plane. $d_A = d_B = d_C = d_D = d_E$.

Consider a 3×3 TX coil array placed 1 *mm* above the center of a $0.2m \times 0.2m \times 0.1m$ solution space as shown in Fig. 5. Assume that the RX and TX coils are parallel to the XY-plane. If positions A, B, C, D and E are in the same XY-plane and have equivalent sum of distances to each TX coil, then evaluating (2) at the five locations yields the same result. In other words, the global fitness values at all these five positions are the same or they are "symmetric" positions in the solution space. More specifically, Fig. 6 shows five typical symmetric scenarios in solution space. A and B are symmetric about the X-axis; A and C are symmetric about the 45^o line; A-D and C-E are symmetric about the origin; A and E are symmetric about the 135^o line. The PSO may fail to find the real position from the symmetric ones, hence positioning failures may occur. These symmetries should not be considered a problem, rather we can exploit them to narrow the optimization space and find the real location of the RX coil more efficiently.

1) Solution space segmentation and selection: As shown in Fig. 7, the solution space is divided into four subspaces, $S1$, $S2$, $S3$ and $S4$, by quadrants of the XY-plane. Due to the non-monotonic nature of the curves in Fig. 2, a certain M between two coils may correspond to two distance values

from one coil to the other. Also, among the distances from the RX coil to the corner coils of the transmit array, the one to the corner coil of the same subspace is the smallest while the one to the corner coil of the diagonal subspace is the largest. Therefore if the $M_{i,meas}$ between the RX coil and one corner TX coil is the largest compared to those between the RX coil and the other three corner TX coils, the RX coil can only be either in the same or diagonal subspace of that particular TX coil. Knowing this, we can run the PSO in those two subspaces only and hence eliminate the potential positioning failure due to the symmetry about axes (e.g. *A* and *B* in Fig. 6).

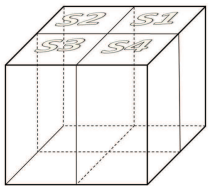

Fig. 7. Segmentation of solution space.

2) TX coils selection: Two selections will be made. First, only the shaded TX coils in Fig. 8(a) are operating when running PSO in the two subspaces identified in the previous step. This combination of operating coils is asymmetric to the 45^o or 135^o line. Furthermore, if we let x be the sum of distances from one point to each operating coil, then this combination is one of the few that have the least number of points giving equal x in the same subspace. Those are the points which may cause positioning failures. Hence this to some extent breaks the symmetry in the same subspace (e.g. *A* and *C* or *D* and *E* in Fig. 6). Second, after two possible locations are identified in two diagonal subspaces, the $M_{i,meas}$ corresponding to selected coils shown in Fig. 8(b) are compared with their respective $M_{i,calc}$, the location giving the smallest sum of difference between the $M_{i,meas}$ and the $M_{i,calc}$ of selected coils will be the final estimated location of the RX coil. This new combination of coils breaks the symmetry about the origin (e.g. *A* and *D* or *C* and *E* in Fig. 6) since it doesn't contain any two coils symmetric about the origin. Other combinations having the same property will work as well.

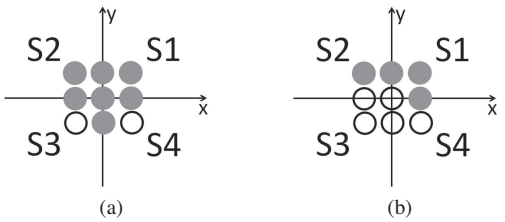

Fig. 8. Shaded coils are the operating TX coils in (a) first round of coils selection; (b) second round of coils selection.

D. Simulation results

The MATLAB simulation results are shown in Table I. Eighty particles are used in each subspace. The positioning error is defined in (5) where the subscripts *est* and *true* denote the estimated and real location of the RX coil respectively. The algorithm has been tested when the RX coil is placed at 1000 locations randomly drawn from all possible locations uniformly distributed in the solution space. Table I shows that 92.6% of the positioning errors are within 1 *mm*. However, for 0.4% of the time the positioning errors are greater than 5 *cm* which is much larger than the rest. They are considered as positioning failures. Improving the algorithm to completely eliminate those failures is included in future work of this project.

$$\sqrt{(x_{est}-x_{true})^2+(y_{est}-y_{true})^2+(z_{est}-z_{true})^2} \qquad (5)$$

TABLE I
POSITIONING ERROR DISTRIBUTION

Error range	Percentage
$\leq$1 *mm*	92.6%
$\geq$ 5 *cm*	0.4%

IV. CONCLUSION

This paper presents a novel implant positioning system based on mutual inductance. The theory and feasibility of this scheme have been demonstrated via a lookup table approach. A positioning algorithm based on a modified Particle Swarm Optimizer is used to exploit the symmetry of spatial variation of mutual inductance with the relative position of the RX coil and the TX coil array. MATLAB simulation of this algorithm showed a positioning accuracy within sub-millimeter range for 92.6% of the time. On-going work includes improving positioning algorithm accuracy and designing a power efficient hardware realization of the implant position system. We believe that this new scheme is promising for locating and directing wireless power to a wide range of *mm*-sized implantable devices.

REFERENCES

[1] C. Hu, M.-H. Meng, M. Mandal, and X. Wang, "3-axis magnetic sensor array system for tracking magnet's position and orientation," in *Intelligent Control and Automation, 2006. WCICA 2006. The Sixth World Congress on*, 0 2006.

[2] D. D.Fischer, R.Schreiber and R.Eliakim, "Capsule endoscopy: the localization system," *Gastronintestinal endoscopy clinics of North America*, vol. 14, pp. 25–31, 2004.

[3] G. X.Guo and W. He, "A position telemetric method for implantable microcapsules in the gastrointestinal tract," *Measurement Science and Technology*, vol. 19, no. 4, 2008.

[4] S. O'Driscoll, A. Poon, and T. Meng, "A mm-sized implantable power receiver with adaptive link compensation," in *Solid-State Circuits Conference - Digest of Technical Papers, 2009. ISSCC 2009. IEEE International*, pp. 294 –295,295a, feb. 2009.

[5] C. Hu, M. Q. Meng, and M. Mandal, "Efficient magnetic localization and orientation technique for capsule endoscopy," in *Intelligent Robots and Systems, 2005. (IROS 2005). 2005 IEEE/RSJ International Conference on*, pp. 628 – 633, aug. 2005.

[6] J. Kennedy and R. Eberhart, "Particle swarm optimization," in *Neural Networks, 1995. Proceedings., IEEE International Conference on*, vol. 4, pp. 1942 –1948 vol.4, nov/dec 1995.